ALTERNATIVE ENERGY

Ultrastretchable, transparent triboelectric nanogenerator as electronic skin for biomechanical energy harvesting and tactile sensing

Xiong Pu,[1]* Mengmeng Liu,[1]* Xiangyu Chen,[1] Jiangman Sun,[1] Chunhua Du,[1] Yang Zhang,[1] Junyi Zhai,[1] Weiguo Hu,[1†] Zhong Lin Wang[1,2†]

Rapid advancements in stretchable and multifunctional electronics impose the challenge on corresponding power devices that they should have comparable stretchability and functionality. We report a soft skin-like triboelectric nanogenerator (STENG) that enables both biomechanical energy harvesting and tactile sensing by hybridizing elastomer and ionic hydrogel as the electrification layer and electrode, respectively. For the first time, ultrahigh stretchability (uniaxial strain, 1160%) and transparency (average transmittance, 96.2% for visible light) are achieved simultaneously for an energy-harvesting device. The soft TENG is capable of outputting alternative electricity with an instantaneous peak power density of 35 mW m^{-2} and driving wearable electronics (for example, an electronic watch) with energy converted from human motions, whereas the STENG is pressure-sensitive, enabling its application as artificial electronic skin for touch/pressure perception. Our work provides new opportunities for multifunctional power sources and potential applications in soft/wearable electronics.

INTRODUCTION

The past decade has witnessed the rapid growth of flexible/stretchable electronics, with the advent of various revolutionary multifunctional devices ranging from flexible transistors (*1*, *2*) and integrated circuits (*3*, *4*), stretchable luminescence devices (*5*, *6*), and roll-up displays (*7*) to smart sensor-integrated electronic skins (*8*–*10*). These advancements impose the challenge on corresponding power devices that they should have comparable flexibility/stretchability. For example, stretchable and transparent actuator (*11*) and touch panel (*12*) have been recently demonstrated, but no reported energy device can simultaneously achieve the high transparence and stretchability. Meanwhile, the growing wearable consumer electronics, either integrated in clothes/wears or attached on or implanted in curved human body, rely on power devices that are stretchable, shape-adaptive, and biocompatible.

Because of the intrinsic energy conversion mechanism, it is hard for some energy harvesters to achieve high stretchability, for example, the strong magnetic field required for conventional electromagnetic generator; on the contrary, the recently developed triboelectric nanogenerator (TENG) is naturally flexible and has potential for high stretchability (*13*–*16*). The TENG, converting mechanical energy into electricity based on the coupling effect of contact electrification and electrostatic induction, has been demonstrated to be versatile in harvesting different types of energies and has the advantages of simple structure, vast material choice, and low cost (*17*–*22*). Several stretchable TENGs have been recently reported (*23*–*28*) with similar strategy as most reported stretchable devices, which are enabled by anchoring percolated networks of conductive materials (carbon nanotubes, graphene, carbon paste, silver nanowires, etc.) on prestrained elastomer substrates. However, the stretchability or ultimate strain (ε_{ult}) for this strategy is limited, typically below the ultimate strain of the elastomer (for example, 400 to 700% for silicones), due to the markedly increased sheet resistance when being stretched and the loss of percolation at large strain. Another recently reported stretchable TENG achieved ~300% tensile strain by using water or ionic liquid as the electrode, but its application is limited by the use of liquid materials (*29*).

Hydrogels, composed of hydrophilic polymer networks swollen with water or ionic aqueous solution, are in solid form, soft, stretchable (ε_{ult}, ~2000%), and biocompatible (*30*). Some hydrogels are transparent in full visible spectrum (*11*). Meanwhile, the increments of their resistivity with strain are orders of magnitude lower than those of percolated conductive networks (*11*). Many stretchable functional devices have been demonstrated with ionic hydrogels as the electrode conductors, such as strain sensors (*31*), loudspeakers (*11*), and electroluminescent devices (*32*).

Here, we report a soft skin-like TENG (STENG) that enables both biomechanical energy harvesting and touch sensing by using elastomer and ionic hydrogel as the electrification layer and electrode, respectively. Different from previously reported TENGs using electrical conductors as the electrode, this soft STENG uses ionic conductors as the electrode. Polyacrylamide (PAAm) hydrogel containing lithium chloride (LiCl) is used as the ionic hydrogel (PAAm-LiCl hydrogel), and two commonly used elastomers, that is, polydimethylsiloxane (PDMS) Sylgard 184 and 3M VHB 9469, are adopted. For the first time, ultrahigh stretchability (ultimate stretch λ of up to 12.6 or strain ε of 1160%) and high transparency (up to 96.2%) are achieved simultaneously for an energy device because all engaged materials are stretchable and transparent. These soft skin-like generators are capable of outputting an open-circuit voltage of up to 145 V and an instantaneous areal power density of 35 mW m^{-2}. Meanwhile, the STENG-based electronic skin can sense pressure of as low as 1.3 kPa. The current study presents an energy harvester that is superstretchable, biocompatible, and transparent for the first time, allowing energy generation and touch sensing without interference of optical information's delivering and could thus have potential in smart artificial skins, soft robots, functional displays, wearable electronics, etc.

RESULTS

A sandwich-like architecture was adopted for the design of the STENG, as illustrated in Fig. 1A. The PAAm-LiCl hydrogel was sealed

[1]Beijing Institute of Nanoenergy and Nanosystems, Chinese Academy of Science, National Center for Nanoscience and Technology, Beijing 100083, China. [2]School of Materials Science and Engineering, Georgia Institute of Technology, Atlanta, GA 30332–0245, USA.
*These authors contributed equally to this work.
†Corresponding author. Email: huweiguo@binn.cas.cn (W.H.); zhong.wang@mse.gatech.edu (Z.L.W.)

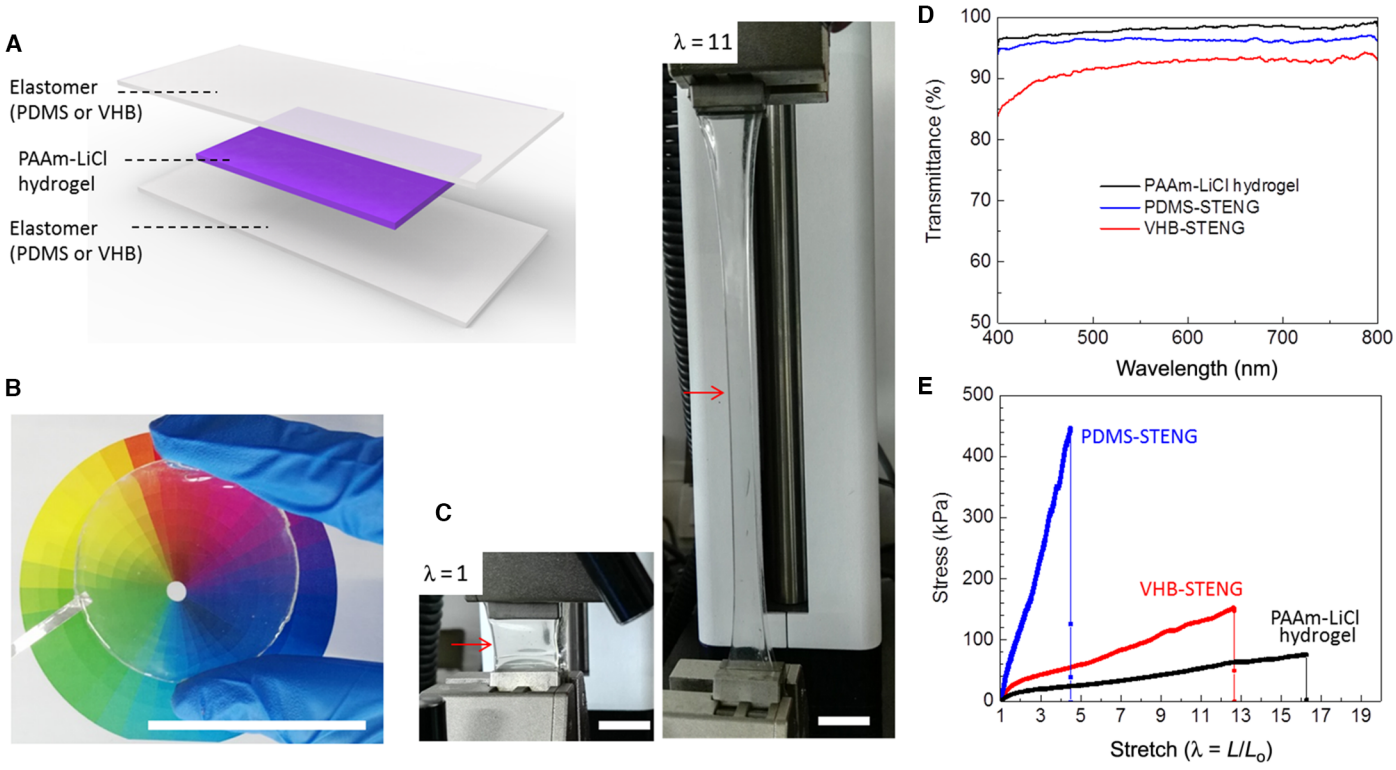

Fig. 1. The design of transparent and superstretchable STENG. (**A**) Scheme of the STENG with sandwich structure. (**B**) A circular STENG that is transparent to full visible colors. (**C**) VHB-STENG (indicated by arrows) at initial state (stretch λ = 1) and stretched state (λ = 11 or strain ε = 1000%). (**D**) Transmittance in the visible range and (**E**) uniaxial tensile test of the PAAm-LiCl hydrogel, PDMS-STENG, and VHB-STENG. Scale bars, 5 cm (B) and 15 mm (C).

between two elastomer films, and an Al belt or a Cu wire was attached to the hydrogel for electrical connection. Commercial PDMS or VHB was used as the elastomer film, denoted as PDMS-STENG and VHB-STENG, respectively. For the convenience of handling, the thickness of the hydrogel film is controlled to be about 2 mm; the thickness of PDMS and VHB is about 90 and 130 μm, respectively. The final devices can be of arbitrary two-dimensional shapes. Figure 1B shows an image of a circular PDMS-STENG that is highly transparent to all visible colors. Because all engaged elastomers and PAAm-LiCl hydrogel are stretchable, the final device is ultrastretchable as well, as confirmed by the image (Fig. 1C) of a VHB-STENG at initial state (stretch $\lambda = L/L_o = 1$) and after being uniaxially stretched for 11 times (stretch λ = 11 or strain ε = 1000%). The images of a PDMS-STENG with uniaxial stretch λ = 4 and a PAAm-LiCl hydrogel with stretch λ = 15 are also shown in fig. S1.

The 2-mm-thick PAAm-LiCl hydrogel achieves an average transmittance of 98.2% (Fig. 1D) in the visible range (wavelength, 400 to 800 nm), which is less transparent than that of the previously reported 11-mm-thick PAAm-NaCl hydrogel (98.9%) due to the higher salt concentration in the current study (8 M) (*11*). The PDMS-STENG and VHB-STENG show average transmittances of 96.2 and 91.9%, respectively, both much higher than those of previously reported transparent TENG using graphene or indium tin oxide (ITO) (*33*–*36*). Uniaxial tensile tests are performed to evaluate the mechanical properties of the hydrogels and STENGs (Fig. 1E). The PAAm-LiCl hydrogel shows an ultimate stress of 75.8 kPa at a stretch of λ = 16.2; whereas the VHB-STENG ruptures at a stress of 152.4 kPa and a stretch of 12.6, the PDMS-STENG ruptures at a stress of 446.2 kPa and a stretch of 4.5. It therefore can be suggested that the stretchability and strength of the STENGs are tunable by selecting appropriate elastomer/hydrogel combinations for specific requirements and that ultrahigh stretchability and transparency have been achieved simultaneously.

There are generally four types of working modes for a TENG, that is, contact-separation mode, sliding mode, freestanding mode, and single-electrode mode (*37*). If the PAAm-LiCl hydrogel is connected to the ground by a metal wire through the external load, the STENG will work in the single-electrode mode (Fig. 2A). Once an object (typically dielectric materials different from the elastomer) contacts with the elastomer film of the STENG, electrification occurs at the interface and generates the same amount of charges with opposite polarities at the surface of the dielectric film and the elastomer, respectively (Fig. 2A, i). Because the two opposite charges coincide at almost the same plane, there is practically no electrical potential difference between the two surfaces. When the two surfaces are separating and moving away, the static charges on the surface of the insulating elastomer will induce the movement of the ions in the ionic hydrogel to balance the static charges, forming a layer of excessive ions (positive in the example in Fig. 2A, ii) at the interface. Meanwhile, the electrical double layer formed at the metal/electrolyte (that is, ionic hydrogel) interface will be polarized, forming the same amount of excessive negative ions at the interface and positive charges in the metal wire (Fig. 2A, v). To achieve this double layer, electrons flow from the metal wires to the ground through the external circuits until all the static charges in the elastomer film are screened (Fig. 2A, iii). If the moving dielectric film is approaching back to the elastomer film, the whole process will be reversed and an electron flux with the opposite direction will transfer

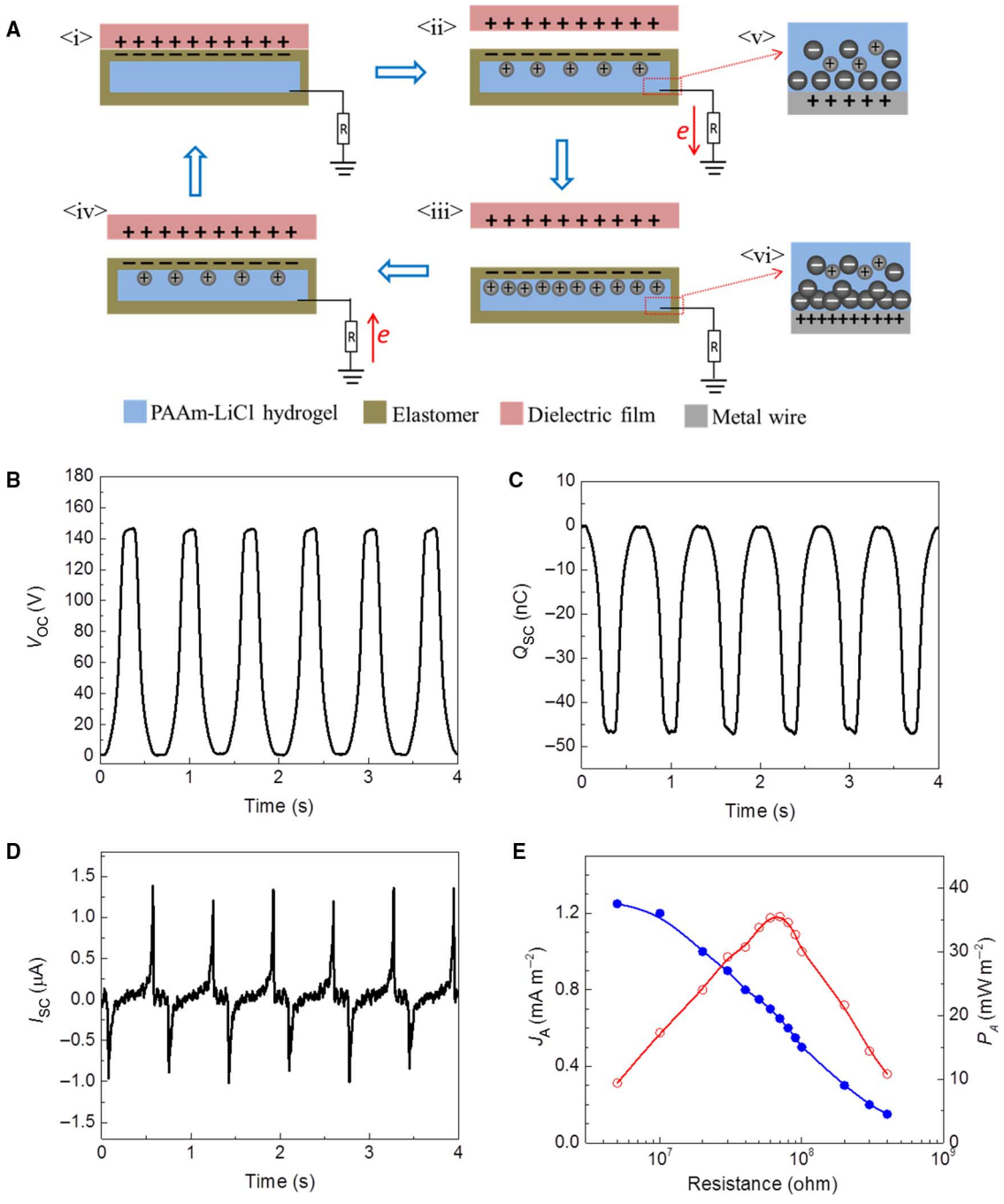

Fig. 2. The working principles and output characteristics of the STENG at single-electrode mode. (**A**) Scheme of the working mechanism of the STENG. (**B**) Open-circuit voltage V_{OC} (B), (**C**) short-circuit charge quantity Q_{SC}, and (**D**) short-circuit current I_{SC} of a PDMS-STENG. (**E**) Variation of the output current density and power density with the external loading resistance.

from the ground to the metal/hydrogel interface through the external load (Fig. 2A, iv). By repeating the contact-separation movement between the dielectric object and the STENG, an alternative current will be generated.

The electrical double layer formed at the metal/hydrogel interface has a thickness typically in the nanometer range, which leads to a high capacitance (c_{EDL} is in the order of 0.1 F m^{-2}) (*11*, *38*). The contacting area (A_{EDL}) of the metal wire and the hydrogel is in the order of ~10 mm^2, and the quantity of transferred charges (Q) is in the order of ~10 nC (the data will be presented in later discussions). Then, the voltage across the electrical double layer ($V_{EDL} = Q/Ac_{EDL}$) is in the order of ~10^{-2} V. Therefore, the metal/hydrogel interface is stable, and no electrochemical reaction will happen because the voltage is well below 1 V (*11*).

STENG fundamentally has inherent capacitive behavior because it is an electrostatic system, and it can be equivalent to a circuit consisting of a series of capacitors, as shown in fig. S2. The output voltage under

open-circuit condition (V_{OC}) and the transferred charges under short-circuit condition (Q_{SC}) have a relationship of (*37*, *39*)

$$Q_{SC} = V_{OC}C_o \quad (1)$$

where C_o is the capacitance of the STENG. When the moving dielectric film is in contact with the elastomer, V_{OC} and Q_{SC} are both 0. When the dielectric film is moving far away, V_{OC} and Q_{SC} can be derived as (see detailed explanations in fig. S2) (*37*, *39*)

$$V_{OC} = -\sigma A/2C_o \quad (2)$$

$$Q_{SC} = -\sigma A/2 \quad (3)$$

where σ is the density of electrostatic charges generated at the surface of the elastomer film and A is the contacting area between the dielectric film and the elastomer film.

To measure the output of the STENG, we used a commercial Nylon film to have contact-separation movement relative to a PDMS-STENG (area, 3 × 4 cm). Other than mentioned, the frequency (1.5 Hz) and speed (0.2 m s^{-1}) of the contact-separation motion and the pressure (~100 kPa) between the two contacting films are all controlled to be the same by a stepping motor for all following tests. The peak V_{OC} and the peak Q_{SC} are about 145 V (Fig. 2B) and 47 nC (Fig. 2C), respectively. Under short-circuit conditions, an alternative current was measured with a peak value of ~1.5 μA (Fig. 2D). By varying the external resistance, the maximum output areal power density was measured to be ~35 mW m^{-2} at a matched resistance of ~70 megohm (Fig. 2E). Similar output characteristics were obtained for the VHB-STENG (fig. S5).

The STENG can also work at a two-electrode contact-separation mode, as shown in fig. S6. Different from the single-electrode mode, the moving dielectric film is replaced with a second metal electrode that is connected to the PAAm-LiCl hydrogel through the external circuit (fig. S6A). When Al foil was used as the second electrode, the generated peak V_{OC} and peak Q_{SC} are about 182 V (fig. S6B) and 130 nC (fig. S6C), respectively. The instantaneous peak value of the ac current is around ~20 μA (fig. S6D), and a maximum areal power density of ~328 mW m^{-2} can be reached at a loading resistance of ~7 megohm (fig. S6E).

Because of the universality of contact electrification between any two different materials, the STENG can generate voltage/current outputs from the relative motion between the STENG and many other materials. A series of materials were used to have contact-separation motion relative to the STENG in single-electrode mode, and corresponding open-circuit voltages were recorded (Fig. 3A and fig. S7). The amplitude and polarization of V_{OC} depend on the relative ability of a material to lose or gain electrons when contacting with the elastomer. Compared with VHB (typically acrylate polymers), all of Nylon (polyamide), latex, silk, paper, Al, cotton, and polyester (PET) are tending to lose electrons and therefore are more tribo-positive, whereas Kapton (polyimide) and PDMS are more tribo-negative and the polarization of the V_{OC} is reversed (Fig. 3, A and B), coincident with the well-established tribo-series table (*18*, *40*). The larger the difference in the ability of losing/gaining electrons between the two contacting materials, the more electrostatic charges generated at the interface and thus the higher output V_{OC}. Nylon and

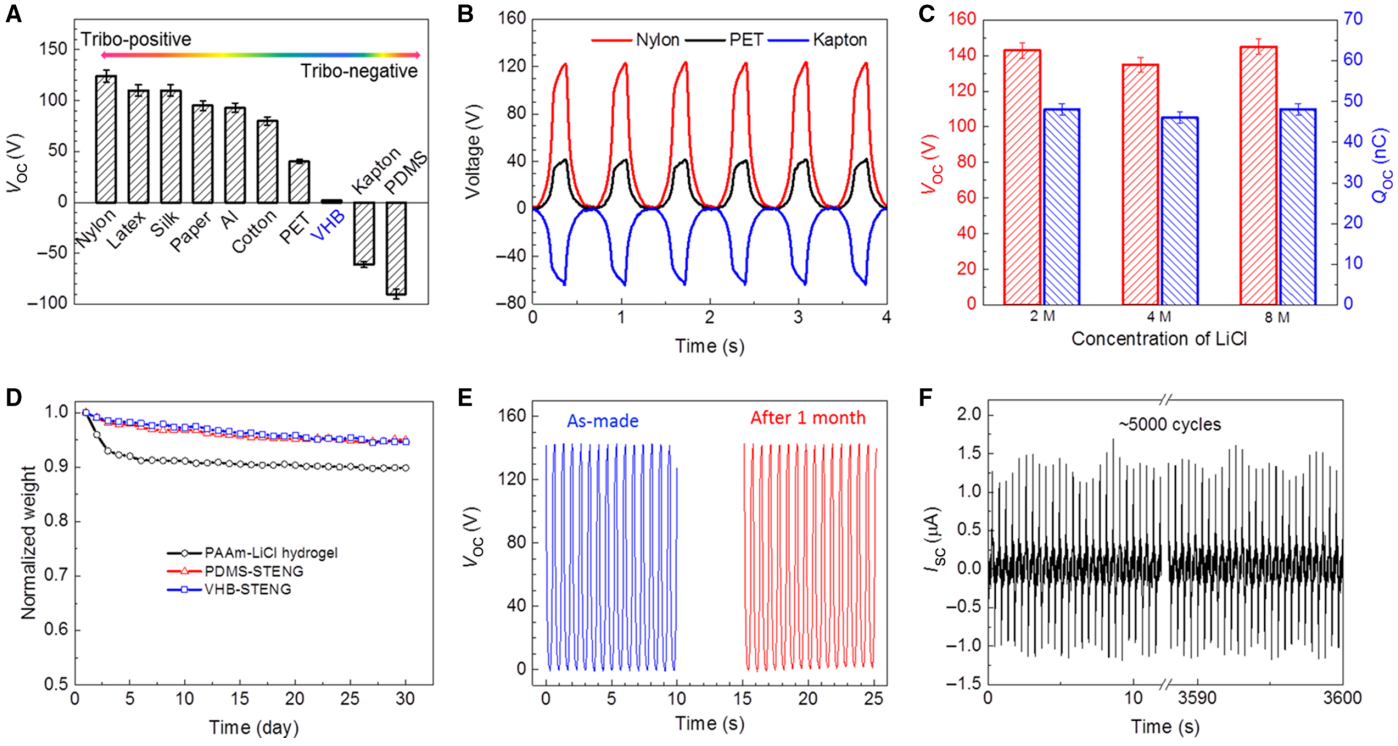

Fig. 3. The material choices and durability of the STENG. (**A**) Summarized peak amplitude (A) of V_{OC} and (**B**) three representative V_{OC} profiles (B) of a VHB-STENG with relative contact-separation motion to different materials. (**C**) Output V_{OC} and Q_{SC} of a PDMS-STENG using PAAm-LiCl hydrogel with different LiCl concentrations. (**D**) Normalized weight retention of the PAAm-LiCl hydrogel, VHB-STENG, and PDMS-STENG kept at a dry environment with an RH of 30% at 30°C. (**E**) Comparison of the V_{OC} of the PDMS-STENG before and after storing in the dry environment for 30 days. (**F**) I_{SC} of a PDMS-STENG that lasted for ~5000 cycles of contact-separation motions (1 hour).

PDMS are the most tribo-positive and tribo-negative among tested materials, respectively. Consistent results are also obtained when using PDMS as the elastomer film for the PDMS-STENG (fig. S7), where all tested materials are more tribo-positive than PDMS. Because PDMS is more tribo-negative than VHB, the PDMS-STENG has relatively larger output than that of VHB-STENG when the same materials were used for the contact-separation motion. Human skin can also be used to have contact separation with the STENG. As shown in fig. S8, current can be generated when using a hand to tap a PDMS-STENG with or without a latex glove. The viability of the STENG in relative motion to different materials can make it suitable and applicable for energy harvesting in various applications.

The concentration of the LiCl in the PAAm-LiCl hydrogel was also varied to see its effect on the output performances, but the V_{OC} and Q_{SC} were found to have little dependence on the LiCl concentration (Fig. 3C of a PDMS-STENG). This is easy to understand as far as Eqs. 2 and 3 are considered because the V_{OC} and Q_{SC} are majorly dependent on the generated electrostatic charges, and the concentration of the ionic hydrogel (or electrolyte) will not significantly vary the capacitance of the STENG.

One major concern about hydrogel is the dehydration along with time, which can deteriorate its ionic conductivity and mechanical elasticity. When kept in an environment of an average relative humidity (RH) of ~30% at 30°C, the PAAm-LiCl hydrogel loses water content quickly in the first 3 days (7.1% loss) but stabilizes in the following 27 days, yielding weight retention of 89.8% over a month (Fig. 3D). Whereas the dehydration is greatly alleviated when the PAAm-LiCl hydrogel is sandwiched or sealed with the elastomer films of PDMS and VHB, which have the weight retention of 95.0 and 94.6% after a month in the same environment, respectively, the improved antidehydration capability is mainly because the thin elastomer films can prevent the water evaporation. Despite the slight loss of water content of the PDMS-TENG over a month, the output performances show no noticeable degradation, as confirmed by the comparison between the V_{OC} of the as-made PDMS-STENG in relative motion to a Nylon film and that after storage at an RH of ~30% at 30°C for a month (Fig. 3E). This demonstrated antidehydration performance of the STENG ensures its applicability in many harsh environments.

Because the hydrogel contains large amount of LiCl solution, the STENG can only be applicable in the temperature range between the freezing and boiling point of LiCl solution. Beyond this temperature range, the STENG may be damaged. We tested the performances of the STENG at temperatures ranging from 0° to 80°C. On the basis of our measurements, the V_{OC} and Q_{SC} are stable, other than the small decrease at high temperature at around 60° to 80°C (fig. S9). This is accordant with the previous study that the variation of output is small in the temperature range of 270 to 380 K (*41*). To confirm the thermal durability of the STENG, we further stored the PDMS-STENG, VHB-STENG, and bare hydrogel at different temperatures (0°, 20°, 40°, 60°, and 80°C) for 30 min consecutively. The weight of bare hydrogel decreases significantly when the temperature is more than 40°C, and the shrinkage of the sample can be observed after storing at 60° and 80°C (fig. S10). The weight retention of the hydrogel is only about 68.6% after the test due to the severe water loss at high temperature. However, the hydrogels inside the PDMS-STENG and VHB-STENG can maintain weight retentions of 95.6 and 98.5%, respectively, even after storing at 80°C (fig. S10A), whereas water vapor bubbles inside the PDMS-STENG and VHB-STENG can be observed when the temperature is 80°C. Hence, although the PDMS and VHB films are believed to alleviate the water evaporation of hydrogels, the STENG is believed to be better when used in the temperature range of 0° to 60°C.

Humidity has large effect on the output performances of the STENG (fig. S11). By increasing the humidity, the V_{OC} of both the PDMS-STENG and VHB-STENG decreases significantly. When the RH is about 70%, the V_{OC}s of the PDMS-STENG and VHB-STENG are 20 and 43 V, respectively. In a humid environment, the adsorption of the water molecules will neutralize the surface electrostatic charges so that the output performances of the STENG will be degraded (*17*).

The durability of the STENG was also tested over long-term motion cycles. After ~5000 cycles (for 1 hour) of repeated contact-separation motion of a PDMS-STENG relative to a Nylon film, the short-circuit current shows no obvious degradation (Fig. 3F and fig. S12). An elongated test over ~20000 cycles (for 4 hours) was also conducted to confirm the durability (fig. S12).

One major advantage of hybridizing the elastomer and hydrogel is the high stretchability, as shown in above discussions. The viability of the energy harvesting of the STENG at stretched states was further evaluated. A VHB-STENG (3 cm × 3 cm) was uniaxially stretched for different stretches or strains (Fig. 4A), and corresponding electrical outputs (Fig. 4B) were recorded when having contact-separation motion relative to a dielectric film (that is, a latex film). During the test, the latex film was always maintained to have the similar shape and size as the VHB-STENG. Compared with the initial state without strain ($\lambda = 1$), the open-circuit voltage of the STENG (Fig. 4B) is greatly improved from ~110 to ~180 and ~210 V after being stretched for $\lambda = 3$ and 8, respectively. Similar

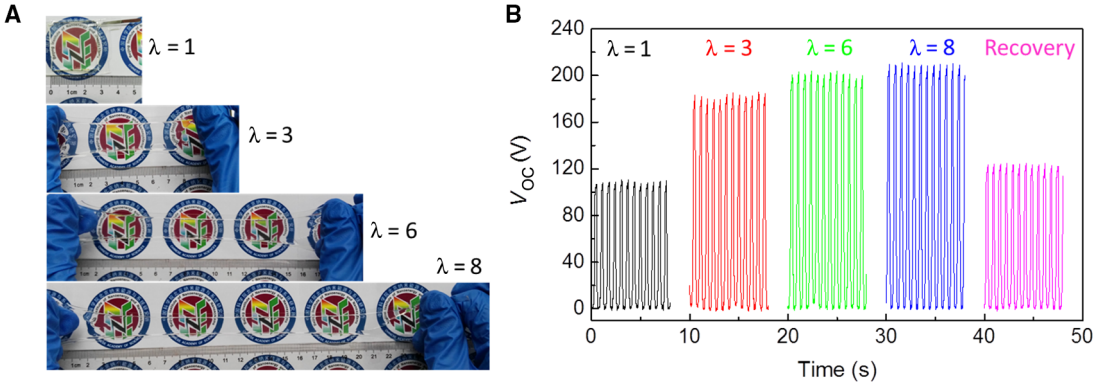

Fig. 4. The stretchability of the STENG. (**A**) Images of a VHB-STENG at initial state and different stretched states and (**B**) its corresponding output V_{OC} (B) when having contact-separation motion to a latex film.

increases in the electrical outputs at stretched states were also observed previously (*23*, *29*). This increment in V_{OC} is attributed to the increase of the surface area of the elastomer film and thus the contacting area for the electrification at stretched states. On the basis of our rough estimation, the area of the STENG is almost doubled after being stretched to $\lambda = 3$. According to Eqs. 2 and 3, both the V_{OC} and Q_{SC} increase when the contacting area A increases. This can also be confirmed by the larger Q_{SC} at stretched states (fig. S13). After recovering from the stretched states, the electrical output is comparable with that at initial state, suggesting no degradation of the device.

For most stretchable devices using percolated networks of carbonaceous materials or metal nanowires, degradation in performances at stretched states is almost inevitable due to the significantly elongated electron transfer paths or even the loss of percolation at large strain. In contrast, the increment in resistance of hydrogel is several orders lower (*11*). Our devices show no degradation but even improvement in the performances at stretched states. Ideally, our devices will work until the mechanical break or fracture of the hydrogel/elastomer; in contrast, the loss of percolation of conductive networks usually happens before the mechanical failure of the substrates. Furthermore, another drawback of the percolated networks is the possible fatigue failure after elongated stretching cycles due to the loss of electrical connection at the network joints. Nevertheless, the STENG with ionic hydrogel as the conductor shows no mechanical fatigue or degradation in electrical output after being stretched for strain $\varepsilon = 200\%$ ($\lambda = 3$) for 1000 cycles (fig. S14). However, note that interface bonding between the PAAm-LiCl hydrogel and the elastomer films is weak because hydrogel is hydrophilic and elastomers are typically hydrophobic. This could be a disadvantage comparing with conductive additive-filled nanocomposites (*42*). For our STENG, the hydrogel is wrapped or sealed inside the elastomer film; it still works after cycles of stretching, but the enhancement in the bonding force can further improve the mechanical durability of the devices. Several recent progresses showed potential approaches to addressing this issue (*43*, *44*).

The STENG can be used for scavenging mechanical energy, especially the energy of human motions. When tapping a transparent VHB-STENG with a hand (with thes human body as the reference electrode or grounding) both at initial and stretched states, 20 green light-emitting diodes (LEDs) connected in series can be easily lighted up (Fig. 5, A and B, and movies S1 and S2). Because the STENG is highly transparent, a VHB-STENG is attached onto a liquid crystal display (LCD) screen, which converts the energy of finger pressing into electricity and powers the screen (Fig. 5C and movie S3). Furthermore, the output of a STENG can be regulated to charge energy storage devices (capacitors or batteries) for powering different portable electronics, as shown by the equivalent circuit in Fig. 5E. For demonstration, a PDMS-STENG was attached on the human skin of the left hand and tapped by the right hand to charge a 2.2-μF capacitor and to power an electronic watch (Fig. 5D). The tapping frequency is about 1 to 2 Hz. In ~160 s, the voltage of the capacitor reaches 4.5 V and can later power the watch for about 15 s (Fig. 5F and movie S4). Subsequently, the capacitor can be charged back to 4.5 V in about 110 to 140 s and can power the watch repeatedly (Fig. 5F). Meanwhile, the STENG, working in two-electrode mode, can charge a Li-ion battery ($LiCoO_2$ as cathode and Li metal as anode) to 3.83 V in 4 hours, which later can be discharged at a constant current of 1 μA for 45 min (fig. S15). Note that the transparent TENG is soft, biocompatible, capable of adapting to the curvy surface of supporting objects in any irregular

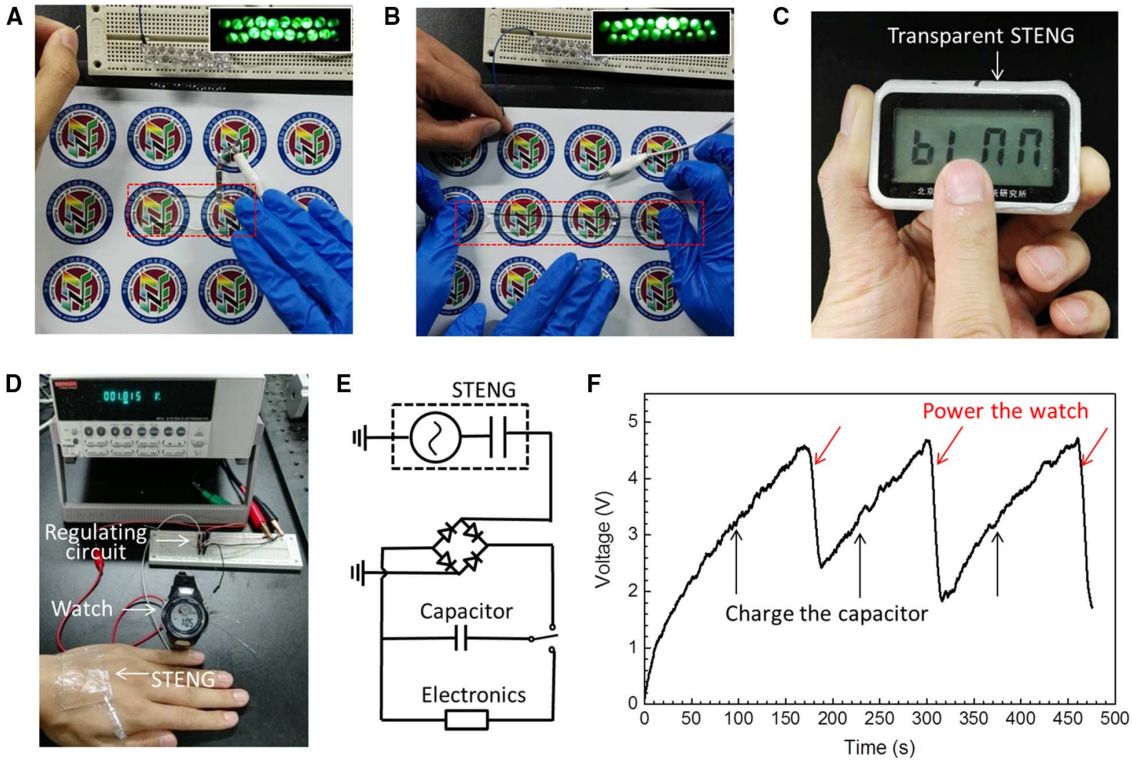

Fig. 5. Biomechanical energy harvesting by the STENG. An image of 20 green LEDs lightened by the VHB-STENG (**A**) at initial state and (**B**) stretched state when being tapped slightly by a hand. (**C**) An image of an LCD screen powered by a transparent VHB-STENG, which covers the screen and converts the energy of finger pressing into electricity. (**D**) An image and (**E**) the equivalent circuit of a self-charging system that uses the energy harvested from the STENG to power electronics (for example, an electronic watch). (**F**) Voltage profile of a 2.2-μF capacitor being charged by the STENG and used to power the electronic watch.

shape and has no interference of the communication of optical information and therefore has high potential in soft robots, foldable touch screens, artificial skins, wearable electronics, etc.

The output of the STENG is also found to be pressure-sensitive in this study and in several previous reports (*45*, *46*). Because the surfaces of the materials always have a certain degree of roughness, the effective contacting area will increase at high pressure because the elastomer and hydrogel are very soft and elastic. The microscale elastic deformation leads to the more intimate contact and more generated electrostatic charges at the interfaces. According to Eqs. 2 and 3, the increase in the electrostatic charge density σ will then raise the output current and voltage. A 20-megohm resistor was connected to a PDMS-STENG (3 × 4 cm), and the voltage drop across the resistor was recorded when pressing a Nylon film onto the PDMS-STENG at different pressures (Fig. 6A). Two reverse voltage peaks were observed, corresponding to the event of touch or separation, respectively (fig. S16). Different from typical pressure sensor, no voltage signal was observed during the time intervals of the touching and separation, although the pressure was still applied on the STENG. However, by increasing the resistance R of the resistor, the measured voltage signals will change to sidestep shape and, finally, to a rectangular shape under open-circuit condition (*45*). The amplitude of the bimodal voltage increases linearly with the pressure when the touch pressure is low and saturates after the pressure is higher than ~70 kPa. The sensitivity (S) is typically defined as $S = (d\Delta V/V_S)/dP$, where ΔV is the relative change of the output voltage, V_S is the saturated voltage, and P is the touch pressure. The calculated sensitivity is 0.013 kPa^{-1}, comparable with that of previously reported TENG-based pressure sensors (*45*) but smaller than many other sensors (*47*). The lowest pressure detection limit is about 1.3 kPa, and the recorded voltages at five different touch pressures are shown in Fig. 6B. The ambient temperature variation has little effect on the sensing properties in the temperature range where the STENG is applicable. As shown in fig. S17, no obvious variation of the voltage was observed in the temperature range of 0° to 80°C. Because the STENG is mainly an electrostatic charge–based capacitive sensor, the temperature-introduced resistance change of the hydrogel will not vary the voltage signal (*48*).

Considering the demonstrated sensing capability of touch and touch pressure, the soft and transparent STENG can be applied as artificial electronic skin. A STENG-based artificial skin with 3 pixel × 3 pixel (each is 1 cm × 1 cm) was fabricated and can be conformally attached onto a curvy hand (Fig. 6C). This artificial skin can perceive the touch by alien objects and the touch pressure. When pressing 1 pixel with a fingertip, the output voltage varies accordingly with the pressure (Fig. 6D). When pressing the sensor arrays with a z-shaped acrylic plate (Fig. 6E), the output voltages can literally represent the touching area of the STENG (Fig. 6F and fig. S18).

DISCUSSION

We reported here a soft STENG composed of a sandwich structure of ionic hydrogels and elastomer films for energy conversion and tactile sensing. These material combinations and structural designs allow the following advantages:

(1) High stretchablity (up to λ = 12.6 or strain ε = 1160%) and transparency (up to 96.2% average transmittance to full spectrum of visible light) are achieved, which are both much higher than those of previously

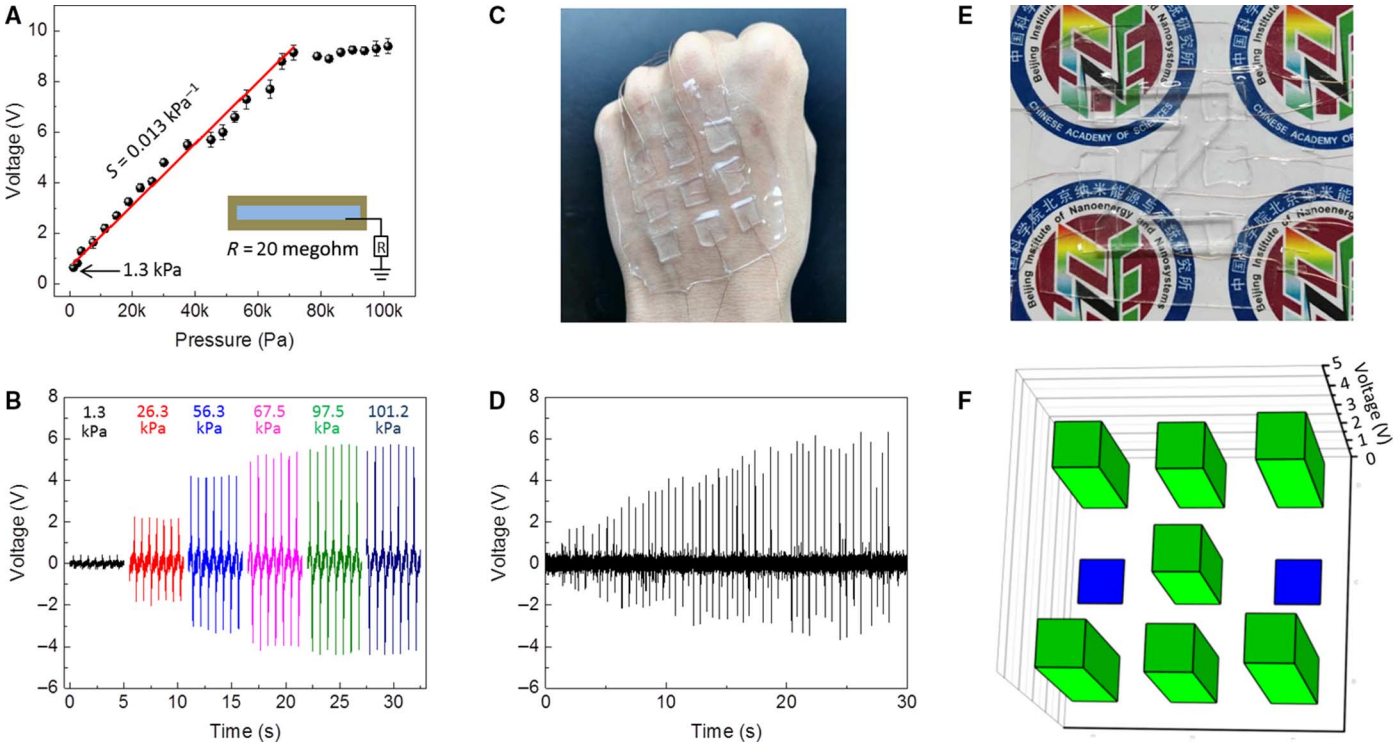

Fig. 6. Tactile sensing by the STENG. (**A**) Summarized variation of peak amplitudes of the voltage across the resistor (20 megohm) with the contact pressure. Inset: Scheme of the STENG-based tactile sensor. (**B**) Representative voltage profiles of the STENG as tactile sensor at five different pressures. (**C**) An image of a STENG-based tactile sensor with 3 pixel × 3 pixel attached on a curvy hand. (**D**) Voltage signals of the tactile sensor by pressing 1 pixel with a finger at increasing pressures. (**E**) An image of the tactile sensor pressed with a z-shaped acrylic plate and (**F**) corresponding voltage signals of the 9 pixels.

reported stretchable and/or energy conversion devices using percolated conductive networks or ITO as the electrode materials (*24*, *29*, *33*, *34*, *36*). No performance degradation is observed at stretched states as well.

(2) The mechanism of STENG is slightly different from that of previously reported TENGs using electrical conductors as the electrode. Ionic conductors (that is, ionic hydrogels) are used, which is demonstrated to be stable and will not be electrolyzed at the interface.

(3) The unique capability of energy harvesting and tactile perception of the STENG may lead to the soft/stretchable self-powered sensors or self-charging power systems in the future (*49*, *50*). For example, self-powered soft robot or electronic skin might be possible in the future by the combination of soft energy-harvesting and energy storage devices and soft sensors and actuators.

(4) Both elastomers and hydrogels are low cost, lightweight, and biocompatible. It is also possible to design the STENG into arbitrary, complicated shapes as long as a thin elastomer film wraps or seals the hydrogels. Meanwhile, the fabrication is facile for scale-up synthesis. Considering the biocompatibility, the STENG has potential for power devices attached on the skin or implanted inside the human body (*51*). Furthermore, both the elastomer and hydrogel have large categories of different materials with various unique properties. The combination of the hydrogel and elastomer has recently led to many multifunctional devices, as mentioned in the Introduction. The STENG with the hydrogel/elastomer combination reported here opens up opportunities for energy generation devices with new functional properties (stretchability, transparency, biocompatibility, etc.) and many potential applications ranging from soft robots, foldable touch screens, and artificial skins, to wearable electronics.

In summary, our approach of soft/stretchable energy harvesting allows the energy conversion from human motions to electricity. The capability of scavenging biomechanical energies of the STENG was demonstrated when applying it as an artificial skin. Capacitors or batteries can be charged by the artificial skin to power wearable electronics. Finally, the sensitivity of the STENG to the input pressure was investigated, which enabled it as an electronic skin for pressure or tactile perception. The applicable temperature of the STENG is optimal at 0° to 60°C; otherwise, the freezing or boiling of the ionic solution in the hydrogel may cause the malfunction of the device. For future research, more multifunctional devices can be explored by developing STENGs with other functional hydrogels/elastomers; the interface bonding between the hydrogel and elastomer should be enhanced to further improve the mechanical performances of the STENG; output performances should be improved by maximizing the surface electrostatic charge density through surface treatments/modifications or materials optimization.

MATERIALS AND METHODS

Materials

Acrylamide, *N*,*N*,*N*′,*N*′-tetramethylethylenediamine, *N*,*N*′-methylenebisacrylamide, ammonium persulfate, and LiCl were from Sigma-Aldrich. Sylgard 184 and VHB film (3M VHB 9469) were used as the elastomer. Lithium foil and $LiCoO_2$ powder were from MTI Corporation.

Fabrication of the PAAm-LiCl hydrogel

The PAAm-LiCl hydrogel was prepared according to the method reported previously. Briefly, acrylamide powder (14 weight % relative to deionized water) was added into 8 M LiCl aqueous solution. Subsequently, *N*,*N*′-methylenebisacrylamide, ammonium persulfate, and *N*,*N*,*N*′,*N*′-tetramethylethylenediamine were dissolved in the solution consecutively. The solution was then transferred into a glass mold and treated in an oven at 50°C for 2 hours to form the PAAm-LiCl hydrogel. The thickness of the final hydrogel was controlled by the volume of the solution. Other than mentioned, all the samples used 8 M LiCl.

Fabrication of the soft TENG

The elastomer VHB film (130 μm thick; 3M VHB 9469) was used as received. The PDMS film was prepared by spin-coating the mixture of Sylgard 184 base and curing agents (10:1 by weight) followed with a 90°C treatment for 1 hour. The PAAm-LiCl hydrogel, VHB, and PDMS were cut into the desired shape with a laser cutter. The final device was fabricated by wrapping and sealing the PAAm-LiCl hydrogel with the elastomer films. An Al belt or a Cu wire was attached to the hydrogel for electrical connection.

Characterization and measurements

A step motor (LinMot E1100) was used to provide the input of mechanical motions. For all the tests of energy generation of the STENG, the pressure (100 kPa), speed (0.2 m/s), and frequency (~1.5 Hz) of the step motor were fixed. The voltage and charge quantity were recorded by a Keithley electrometer 6514, and the current was recorded with a Stanford low-noise preamplifier SR570. The force applied by the motor was detected by a Mark-10 force gauge. The mechanical tensile test and stretch cycling test of the STENGs were conducted by an ESM301/Mark-10 system. For the tensile test, the strain rate was fixed at 40 mm/min. For the antidehydration test, the dry environment was created by storing dehydrated desiccants in an oven at 30°C. The RH was monitored with a hygrometer, and the weights of the samples were recorded everyday. For the measurement of the output performances of the STENG at different temperatures, the STENG was kept inside a thermostat oven (GDW-50L, Wuxi Zhongtian Company), and the contact-separation motion was controlled by the linear motor outside through a feed-through hole. For the measurement of the STENG at different RH, dry air gas carrying water vapor though a water bubbler was introduced into the oven at different flowing rates or a commercial humidifier was used to provide a humid environment. The optical transmittance was measured by a Shimadzu UV-3600 spectrophotometer. A Li-ion battery was assembled with commercial $LiCoO_2$ (MTI Corporation) as the cathode and Li metal as the anode. Before the battery charging by the STENG, the $LiCoO_2$-Li battery was discharged to 3.5 V at a current of 1 μA repeatedly for three times to deplete the residual capacity. The discharge of the battery was conducted by a battery cycler (LAND CT2001A).

SUPPLEMENTARY MATERIALS

Supplementary material for this article is available at http://advances.sciencemag.org/cgi/content/full/3/5/e1700015/DC1

fig. S1. The images of the stretchable PDMS-STENG and hydrogel.
fig. S2. The explanation of the working mechanism of the STENG.
fig. S3. The scanning electron microscopy image of the surface of PDMS and VHB.
fig. S4. The images of the PDMS-STENG and VHB-STENG folded completely.
fig. S5. The output characteristics of a VHB-STENG at single-electrode mode.
fig. S6. The working mechanism and output characteristics of the STENG at two-electrode mode.
fig. S7. Material choices of the PDMS-STENG.
fig. S8. Rectified current output of the STENG by hand tapping.
fig. S9. Temperature effect on the performances of the STENG.
fig. S10. Thermal durability of the STENG.
fig. S11. Humidity effect on the performances of the STENG.
fig. S12. The durability of the STENG.
fig. S13. The Q_{SC} of a VHB-STENG at initial state and different stretched states.
fig. S14. Stretching cycling test of the STENG.
fig. S15. Battery charging by the STENG.

fig. S16. The difference between the V_{OC} and the voltage across the resistor.
fig. S17. Temperature effect on the sensing properties of the STENG.
fig. S18. Voltages of the 9 pixels when pressing the sensor matrix with a z-shaped acrylic plate.
movie S1. Hand-tapping energy harvesting of a VHB-STENG at initial state.
movie S2. Hand-tapping energy harvesting of a VHB-STENG at stretched state.
movie S3. Powering an LCD screen by a transparent VHB-STENG.
movie S4. Powering an electronic watch with the energy converted from hand tapping by a PDMS-STENG.

REFERENCES AND NOTES

1. B. Tian, T. Cohen-Karni, Q. Qing, X. Duan, P. Xie, C. M. Lieber, Three-dimensional, flexible nanoscale field-effect transistors as localized bioprobes. *Science* **329**, 830–834 (2010).
2. T. Sekitani, U. Zschieschang, H. Klauk, T. Someya, Flexible organic transistors and circuits with extreme bending stability. *Nat. Mater.* **9**, 1015–1022 (2010).
3. D.-H. Kim, J.-H. Ahn, W. M. Choi, H.-S. Kim, T.-H. Kim, J. Song, Y. Y. Huang, Z. Liu, C. Lu, J. A. Rogers, Stretchable and foldable silicon integrated circuits. *Science* **320**, 507–511 (2008).
4. D.-m. Sun, M. Y. Timmermans, Y. Tian, A. G. Nasibulin, E. I. Kauppinen, S. Kishimoto, T. Mizutani, Y. Ohno, Flexible high-performance carbon nanotube integrated circuits. *Nat. Nanotechnol.* **6**, 156–161 (2011).
5. M. S. White, M. Kaltenbrunner, E. D. Glowacki, K. Gutnichenko, G. Kettlgruber, I. Graz, S. Aazou, C. Ulbricht, D. A. M. Egbe, M. C. Miron, Z. Major, M. C. Scharber, T. Sekitani, T. Someya, S. Bauer, N. S. Sariciftci, Ultrathin, highly flexible and stretchable PLEDs. *Nat. Photonics* **7**, 811–816 (2013).
6. J. Liang, L. Li, X. Niu, Z. Yu, Q. Pei, Elastomeric polymer light-emitting devices and displays. *Nat. Photonics* **7**, 817–824 (2013).
7. L. Zhou, A. Wanga, S.-C. Wu, J. Sun, S. Park, T. N. Jackson, All-organic active matrix flexible display. *Appl. Phys. Lett.* **88**, 083502 (2006).
8. S. C. B. Mannsfeld, B. C.-K. Tee, R. M. Stoltenberg, C. V. H.-H. Chen, S. Barman, B. V. O. Muir, A. N. Sokolov, C. Reese, Z. Bao, Highly sensitive flexible pressure sensors with microstructured rubber dielectric layers. *Nat. Mater.* **9**, 859–864 (2010).
9. A. Chortos, J. Liu, Z. Bao, Pursuing prosthetic electronic skin. *Nat. Mater.* **15**, 937–950 (2016).
10. D.-H. Kim, N. Lu, R. Ma, Y.-S. Kim, R.-H. Kim, S. Wang, J. Wu, S. M. Won, H. Tao, A. Islam, K. J. Yu, T.-i. Kim, R. Chowdhury, M. Ying, L. Xu, M. Li, H.-J. Chung, H. Keum, M. McCormick, P. Liu, Y.-W. Zhang, F. G. Omenetto, Y. Huang, T. Coleman, J. A. Rogers, Epidermal electronics. *Science* **333**, 838–843 (2011).
11. C. Keplinger, J.-Y. Sun, C. C. Foo, P. Rothemund, G. M. Whitesides, Z. Suo, Stretchable, transparent, ionic conductors. *Science* **341**, 984–987 (2013).
12. C.-C. Kim, H.-H. Lee, K. H. Oh, J.-Y. Sun, Highly stretchable, transparent ionic touch panel. *Science* **353**, 682–687 (2016).
13. F.-R. Fan, Z.-Q. Tian, Z. L. Wang, Flexible triboelectric generator. *Nano Energy* **1**, 328–334 (2012).
14. F. R. Fan, W. Tang, Z. L. Wang, Flexible nanogenerators for energy harvesting and self-powered electronics. *Adv. Mater.* **28**, 4283–4305 (2016).
15. H. Wu, Y. Huang, F. Xu, Y. Duan, Z. Yin, Energy harvesters for wearable and stretchable electronics: From flexibility to stretchability. *Adv. Mater.* **28**, 9881–9919 (2016).
16. R. Hinchet, W. Seung, S.-W. Kim, Recent progress on flexible triboelectric nanogenerators for selfpowered electronics. *ChemSusChem* **8**, 2327–2344 (2015).
17. Z. Zhao, X. Pu, C. Du, L. Li, C. Jiang, W. Hu, Z. L. Wang, Freestanding flag-type triboelectric nanogenerator for harvesting high-altitude wind energy from arbitrary directions. *ACS Nano* **10**, 1780–1787 (2016).
18. Z. L. Wang, Triboelectric nanogenerators as new energy technology for self-powered systems and as active mechanical and chemical sensors. *ACS Nano* **7**, 9533–9557 (2013).
19. U. Khan, S.-W. Kim, Triboelectric nanogenerators for blue energy harvesting. *ACS Nano* **10**, 6429–6432 (2016).
20. X. Pu, W. Song, M. Liu, C. Sun, C. Du, C. Jiang, X. Huang, D. Zou, W. Hu, Z. L. Wang, Wearable power-textiles by integrating fabric triboelectric nanogenerators and fiber-shaped dye-sensitized solar cells. *Adv. Energy Mater.* **6**, 1601048 (2016).
21. Y. Yu, H. Sun, H. Orbay, F. Chen, C. G. England, W. Cai, X. Wang, Biocompatibility and in vivo operation of implantable mesoporous PVDF-based nanogenerators. *Nano Energy* **27**, 275–281 (2016).
22. X. Pu, L. Li, M. Liu, C. Jiang, C. Du, Z. Zhao, W. Hu, Z. L. Wang, Wearable self-charging power textile based on flexible yarn supercapacitors and fabric nanogenerators. *Adv. Mater.* **28**, 98–105 (2016).
23. Y.-C. Lai, J. Deng, S. Niu, W. Peng, C. Wu, R. Liu, Z. Wen, Z. L. Wang, Electric eel-skin-inspired mechanically durable and super-stretchable nanogenerator for deformable power source and fully autonomous conformable electronic-skin applications. *Adv. Mater.* **28**, 10024–10032 (2016).
24. F. Yi, J. Wang, X. Wang, S. Niu, S. Li, Q. Liao, Y. Xu, Z. You, Y. Zhang, Z. L. Wang, Stretchable and waterproof of self-charging power system for harvesting energy from diverse deformation and powering wearable electronics. *ACS Nano* **10**, 6519–6525 (2016).
25. F. Yi, L. Lin, S. Niu, P. K. Yang, Z. Wang, J. Chen, Y. Zhou, Y. Zi, J. Wang, Q. Liao, Y. Zhang, Z. L. Wang, Stretchable-rubber-based triboelectric nanogenerator and its application as self-powered body motion sensors. *Adv. Funct. Mater.* **25**, 3688–3696 (2015).
26. B.-U. Hwang, J.-H. Lee, T. Q. Trung, E. Roh, D.-I. Kim, S.-W. Kim, N.-E. Lee, Transparent stretchable self-powered patchable sensor platform with ultrasensitive recognition of human activities. *ACS Nano* **9**, 8801–8810 (2015).
27. K. N. Kim, J. Chun, J. W. Kim, K. Y. Lee, J.-U. Park, S.-W. Kim, Z. L. Wang, J. M. Baik, Highly stretchable 2D fabrics for wearable triboelectric nanogenerator under harsh environments. *ACS Nano* **9**, 6394–6400 (2015).
28. X. Chen, X. Pu, T. Jiang, A. Yu, L. Xu, Z. L. Wang, Tunable optical modulator by coupling a triboelectric nanogenerator and a dielectric elastomer. *Adv. Funct. Mater.* **27**, 1603788 (2016).
29. F. Yi, X. Wang, S. Niu, S. Li, Y. Yin, K. Dai, G. Zhang, L. Lin, Z. Wen, H. Guo, J. Wang, M.-H. Yeh, Y. Zi, Q. Liao, Z. You, Y. Zhang, Z. L. Wang, A highly shape-adaptive, stretchable design based on conductive liquid for energy harvesting and self-powered biomechanical monitoring. *Sci. Adv.* **2**, e1501624 (2016).
30. J.-Y. Sun, X. Zhao, W. R. K. Illeperuma, O. Chaudhuri, K. H. Oh, D. J. Mooney, J. J. Vlassak, Z. Suo, Highly stretchable and tough hydrogels. *Nature* **489**, 133–136 (2012).
31. J.-Y. Sun, C. Keplinger, G. M. Whitesides, Z. Suo, Ionic skin. *Adv. Mater.* **26**, 7608–7614 (2014).
32. C. H. Yang, B. Chen, J. Zhou, Y. M. Chen, Z. Suo, Electroluminescence of giant stretchability. *Adv. Mater.* **28**, 4480–4484 (2016).
33. F.-R. Fan, L. Lin, G. Zhu, W. Wu, R. Zhang, Z. L. Wang, Transparent triboelectric nanogenerators and self-powered pressure sensors based on micropatterned plastic films. *Nano Lett.* **12**, 3109–3114 (2012).
34. S. Kim, M. K. Gupta, K. Y. Lee, A. Sohn, T. Y. Kim, K.-S. Shin, D. Kim, S. K. Kim, K. H. Lee, H.-J. Shin, D.-W. Kim, S.-W. Kim, Transparent flexible graphene triboelectric nanogenerators. *Adv. Mater.* **26**, 3918–3925 (2014).
35. Q. Liang, X. Yan, Y. Gu, K. Zhang, M. Liang, S. Lu, X. Zheng, Y. Zhang, Highly transparent triboelectric nanogenerator for harvesting water-related energy reinforced by antireflection coating. *Sci. Rep.* **5**, 9080 (2015).
36. K. Y. Lee, M. K. Gupta, S.-W. Kim, Transparent flexible stretchable piezoelectric and triboelectric nanogenerators for powering portable electronics. *Nano Energy* **14**, 139–160 (2015).
37. S. Niu, Z. L. Wang, Theoretical systems of triboelectric nanogenerators. *Nano Energy* **14**, 161–192 (2015).
38. K. H. Lee, M. S. Kang, S. Zhang, Y. Gu, T. P. Lodge, C. D. Frisbie, "Cut and stick" rubbery ion gels as high capacitance gate dielectrics. *Adv. Mater.* **24**, 4457–4462 (2012).
39. S. Niu, Y. Liu, S. Wang, L. Lin, Y. S. Zhou, Y. Hu, Z. L. Wang, Theoretical investigation and structural optimization of single-electrode triboelectric nanogenerators. *Adv. Funct. Mater.* **24**, 3332–3340 (2014).
40. D. K. Davies, Charge generation on dielectric surfaces. *J. Phys. D Appl. Phys.* **2**, 1533 (1969).
41. X. Wen, Y. Su, Y. Yang, H. Zhang, Z. L. Wang, Applicability of triboelectric generator over a wide range of temperature. *Nano Energy* **4**, 150–156 (2014).
42. J. Park, S. Choi, A. H. Janardhan, S.-Y. Lee, S. Raut, J. Soares, K. Shin, S. Yang, C. Lee, K.-W. Kang, H. R. Cho, S. J. Kim, P. Seo, W. Hyun, S. Jung, H.-J. Lee, N. Lee, S. H. Choi, M. Sacks, N. Lu, M. E. Josephson, T. Hyeon, D.-H. Kim, H. J. Hwang, Electromechanical cardioplasty using a wrapped elasto-conductive epicardial mesh. *Sci. Transl. Med.* **8**, 344ra86 (2016).
43. H. Yuk, T. Zhang, G. A. Parada, X. Liu, X. Zhao, Skin-inspired hydrogel–elastomer hybrids with robust interfaces and functional microstructures. *Nat. Commun.* **7**, 12028 (2016).
44. H. Yuk, T. Zhang, S. Lin, G. A. Parada, X. Zhao, Tough bonding of hydrogels to diverse non-porous surfaces. *Nat. Mater.* **15**, 190–196 (2016).
45. X. Wang, H. Zhang, L. Dong, X. Han, W. Du, J. Zhai, C. Pan, Z. L. Wang, Self-powered high-resolution and pressure-sensitive triboelectric sensor matrix for real-time tactile mapping. *Adv. Mater.* **28**, 2896–2903 (2016).
46. S. W. Chen, X. Cao, N. Wang, L. Ma, H. R. Zhu, M. Willander, Y. Jie, Z. L. Wang, An ultrathin flexible single-electrode triboelectric-nanogenerator for mechanical energy harvesting and instantaneous force sensing. *Adv. Energy Mater.* **7**, 1601255 (2017).
47. L. Pan, A. Chortos, G. Yu, Y. Wang, S. Isaacson, R. Allen, Y. Shi, R. Dauskardt, Z. Bao, An ultra-sensitive resistive pressure sensor based on hollow-sphere microstructure induced elasticity in conducting polymer film. *Nat. Commun.* **5**, 3002 (2014).
48. J. Kim, M. Lee, H. J. Shim, R. Ghaffari, H. R. Cho, D. Son, Y. H. Jung, M. Soh, C. Choi, S. Jung, K. Chu, D. Jeon, S.-T. Lee, J. H. Kim, S. H. Choi, T. Hyeon, D.-H. Kim, Stretchable silicon nanoribbon electronics for skin prosthesis. *Nat. Commun.* **5**, 5747 (2014).
49. Z. L. Wang, Towards self-powered nanosystems: From nanogenerators to nanopiezotronics. *Adv. Funct. Mater.* **18**, 3553–3567 (2008).

50. X. Pu, L. Li, H. Song, C. Du, Z. Zhao, C. Jiang, G. Cao, W. Hu, Z. L. Wang, A self-charging power unit by integration of a textile triboelectric nanogenerator and a flexible lithium-ion battery for wearable electronics. *Adv. Mater.* **27**, 2472–2478 (2015).
51. Q. Zheng, B. Shi, F. Fan, X. Wang, L. Yan, W. Yuan, S. Wang, H. Liu, Z. Li, Z. L. Wang, In vivo powering of pacemaker by breathing-driven implanted triboelectric nanogenerator. *Adv. Mater.* **26**, 5851–5856 (2014).

Acknowledgments
Funding: This study was supported by the "Thousands Talents" program for pioneer researcher and his innovation team, China, National Natural Science Foundation of China (grant nos. 51432005, 61574018, and 51603013), the Youth Innovation Promotion Association of Chinese Academy of Science, the "Hundred Talents Program" of the Chinese Academy of Science, and the National Key Research and Development Program of China (2016YFA0202703). **Author contributions:** X.P. conceived the idea and designed the experiment. W.H. and Z.L.W. guided the project. X.P. and M.L. fabricated the devices and performed measurements. X.P., M.L., W.H., and Z.L.W. analyzed the experimental data, drew the figures, and prepared the manuscript. All authors discussed the results and wrote and commented on the manuscript. **Competing interests:** The authors declare that they have no competing interests. **Data and materials availability:** All data needed to evaluate the conclusions in the paper are present in the paper and/or the Supplementary Materials. Additional data related to this paper may be requested from the authors.

Submitted 20 January 2017
Accepted 31 March 2017
Published 31 May 2017
10.1126/sciadv.1700015

Citation: X. Pu, M. Liu, X. Chen, J. Sun, C. Du, Y. Zhang, J. Zhai, W. Hu, Z. L. Wang, Ultrastretchable, transparent triboelectric nanogenerator as electronic skin for biomechanical energy harvesting and tactile sensing. *Sci. Adv.* **3**, e1700015 (2017).